International Journal of Naval Architecture and Ocean Engineering 13 (2021) 617–627

Contents lists available at ScienceDirect

International Journal of Naval Architecture and Ocean Engineering

journal homepage: http://www.journals.elsevier.com/international-journal-of-naval-architecture-and-ocean-engineering/

Sparse decision feedback equalization for underwater acoustic channel based on minimum symbol error rate

Zhenzhong Wang [a, b], Fangjiong Chen [b, d, *], Hua Yu [b, d], Zhilong Shan [c]

[a] Guangdong Power Communication Technology Co., Ltd., Guangzhou, China
[b] School of Electronic and Information Engineering, South China University of Technology, Guangzhou, China
[c] School of Computer Science, South China Normal University, Guangzhou, China
[d] Key Laboratory of Marine Environmental Survey Technology and Application, Ministry of Natural Resources, Guangzhou, China

ARTICLE INFO

Article history:
Received 31 October 2020
Received in revised form
22 July 2021
Accepted 23 July 2021
Available online 31 July 2021

Keywords:
Underwater acoustic communication
Decision feedback equalization
Minimum symbol error rate (ML)
Turbo receiver

ABSTRACT

Underwater Acoustic Channels (UAC) have inherent sparse characteristics. The traditional adaptive equalization techniques do not utilize this feature to improve the performance. In this paper we consider the Variable Adaptive Subgradient Projection (V-ASPM) method to derive a new sparse equalization algorithm based on the Minimum Symbol Error Rate (MSER) criterion. Compared with the original MSER algorithm, our proposed scheme adds sparse matrix to the iterative formula, which can assign independent step-sizes to the equalizer taps. How to obtain such proper sparse matrix is also analyzed. On this basis, the selection scheme of the sparse matrix is obtained by combining the variable step-sizes and equalizer sparsity measure. We call the new algorithm Sparse-Control Proportional-MSER (SC-PMSER) equalizer. Finally, the proposed SC-PMSER equalizer is embedded into a turbo receiver, which perform turbo decoding, Digital Phase-Locked Loop (DPLL), time-reversal receiving and multi-reception diversity. Simulation and real-field experimental results show that the proposed algorithm has better performance in convergence speed and Bit Error Rate (BER).

1. Introduction

Underwater environment is complicated and time-varying. The underwater acoustic channels usually exhibit severe multipath effects and doppler shifts (Singer et al., 2009). The acoustic signals propagate in water at a speed of about 1500 m per second. They often suffer from multiple reflections and refractions which cause sparse channel impulse responses (Stojanovic and Preisig, 2009). Various channel equalization techniques were proposed to overcome the Inter-Symbol Interference (ISI) caused by multipath effects. By embedding channel equalizer in the receiver, the effect of ISI can be reduced. It is interesting that the sparsity of multipath channels will lead to sparsity of the equalizer (Feng et al., 2012). By taking advantage of this prior information of equalizer sparsity, we will be able to improve the equalization performance.

The study of sparse equalizers has attracted intense research interest (Kocic et al., 1995; Cotter and Rao, 2002; Pelekanakis and Chitre, 2012). Kocic et al. (1995) first proposed a sparse equalization technique based on channel estimation. After the channel was sparsely estimated, the corresponding coefficient vector of equalizer can be calculated. In Cotter and Rao (2002), Cotter et al. illustrated the Match Pursuit (MP) method, which used the residual signal to maximize the correlation operation of the mixed matrix column vector to obtain the estimated sparse channel, and then used the estimated channel to calculate the Decision Feedback Equalizer (DFE). In Pelekanakis and Chitre (2012), Pelekanakis et al. applied the potential Riemannian structure of the channel and used the norm of the channel impulse response value to obtain a differentiable cost function. Then, the cost function was minimized to obtain a sparse estimation of the channel, and the corresponding equalizer was obtained according to the estimated channel.

In order to reduce the degradation of equalization performance caused by inaccurate channel estimation, adaptive equalizers without channel estimation were developed. The Improved

* Corresponding author. School of Electronic and Information Engineering, South China University of Technology, Guangzhou, China.
E-mail address: eefjchen@scut.edu.cn (F. Chen).
Peer review under responsibility of The Society of Naval Architects of Korea.

https://doi.org/10.1016/j.ijnaoe.2021.07.004

Proportionate Normalized Least Mean Square (IPNLMS) (Benesty and Gay, 2002) algorithm, which is developed based on the PNLMS algorithm in Duttweiler (2000), provided an important approach to design equalizers by exploiting the sparsity of the impulse response in echo cancellation. Both PNLMS and IPNLMS algorithms improve the convergence performance of the LMS algorithm by assigning independent steps to the equalizer taps. In Pelekanakis and Chitre (2010), several sparse adaptive filtering algorithms were compared. The simulation results showed that the sparse adaptive filtering algorithm could achieve lower bit error rate and faster convergence speed when the channels are sparse. In Tao et al. (2017), a sparse adaptive algorithm selective zero-attracting normalized LMS (SZA-NLMS) was proposed, which could improve the convergence speed of the equalizer by combining data reuse and Multiple-Input Multiple-Output (MIMO) technique. Liu et al. (2017) used a variety of norms as sparse constraints to derive a series of Least Absolute Shrinkage and Selection Operator Recursive Least Squares (LASSO RLS).

The algorithms mentioned above are based on the Minimum Mean Square Error (MMSE) criterion. However, experimental analysis shows that the system does not necessarily achieve the Minimum Symbol Error Rate (MSER) when minimum MSE is reached (Chen et al., 2008). In communication systems, we concerned about the symbol error rate more than the MSE. In recent decades, MSER based equalization techniques have been investigated (Chen et al., 2004, 2006; Gong et al., 2013; Zheng et al., 2013; Xu et al., 2018). In (Gong et al., 2013) a simpler adaptive MSER equalization algorithm was derived by minimizing the Euclidean distance of the equalizers between two time-slots. Linear and decision feedback equalizers based on adaptive MSER have been proposed (Zheng et al., 2013). In Xu et al. (2018), the MSER equalization technique was applied to the underwater acoustic receiver, and showed satisfactory performance. However, the adaptive MSER equalizer suffers from slow convergence. By using sparsity of equalizer, in this paper we shall show that the equalizer performance can be further improved.

It is worth noting that the turbo equalization technology has been applied in underwater acoustic communication systems. In order to utilize the equalizer sparsity, Qingwei et al. (2012) introduced a technique that combines the IPNLMS algorithm with multi-channel turbo equalization. The results of lake test show that the proposed algorithm can reach 2kbps data rate transmission under 1.8 km range, 2 kHz bandwidth. Duan et al. (2017) applied the IPNLMS algorithm to adaptive turbo equalization, and in combination with MIMO technology, faster convergence could be achieved with fewer training sequences. Wu et al. (2015) designed a scheme that used multiple thresholds to determine the linear equalizer tap position and reused the training sequence in the turbo iteration. By adopting the sparse filtering algorithm in turbo equalization, the performance of underwater acoustic communication system has been significantly improved.

This paper is inspired by Yukawa and Yamada (2009); Das and Chakraborty, 2016), and is the first time to combine the sparse precessing with the MSER equalization. Compared with the original MSER equalizers, our proposed scheme adds sparse matrix to the iterative formula which can assign independent steps to the equalizer taps. We also propose a selection scheme for the sparse matrix, so as to guarantee fast convergence of the proposed adaptive equalizer. Finally, we propose a receiver structure that combines our proposed algorithm with turbo decoding, digital phase-locked loop, time reversal and multi-reception diversity. The effectiveness of the proposed algorithm is verified by simulated channel and real-field experiment in the Thousand island Lake.

The rest of this paper is arranged as follows. Section 2 describes the system model used in the derivation algorithm. Section 3 deduces the sparse MSER equalization algorithm under 4QAM sources. Section 4 expounds the determination of sparse matrix elements and proposes a sparse matrix selection scheme. Section 5 introduces the proposed receiver structure. Section 6 verifies our algorithm by simulation. Finally, Section 7 concludes this paper.

2. System model

We consider a time-invariant channel denoted as $h_k(k = 0, \ldots, L-1)$, where L is the length of channel responses. When the transmitted symbols s_k pass through the channel, we can get

$$r_k = \sum_{l=0}^{L-1} h_l s_{k-l} + n_k, \tag{1}$$

where n_k is the channel noise, r_k is the received signal. The received signal can be presented in vector-matrix form as

$$\mathbf{r}_k = \mathbf{H}\mathbf{s}_k + \mathbf{n}_k, \tag{2}$$

where $\mathbf{r}_k = [r_k, r_{k-1}, \ldots, r_{k-N_{f-1}}]^T$ with N_{f-1} being an integer indicating the vector length, $\mathbf{H}$ is the Toeplitz matrix composed of the channel impulse response and $\mathbf{s}_k = [s_k, \ldots, s_{k-L-N_f-1}]^T$ is the transmitted symbol vector, and $\mathbf{n}_k = [n_k, \ldots, n_{k-L-N_f-1}]^T$. The output of a decision feedback equalizer is given by Zheng et al. (2013)

$$y_k = \mathbf{w}_k^T \mathbf{r}_k + \mathbf{b}_k^T \hat{\mathbf{s}}_k, \tag{3}$$

where $\mathbf{w}_k = [w_{k,0}, w_{k,1}, \ldots, w_{k,N_{f-1}}]^T$, $\mathbf{b}_k = [b_{k,0}, b_{k,1}, \ldots, b_{k,N_{b-1}}]^T$ denotes respectively the forward and backward filtering coefficients at time slot k. $\hat{\mathbf{s}}_k = [\hat{s}_{k-D-1}, \hat{s}_{k-D-2}, \ldots, \hat{s}_{k-D-N_b}]^T$ is the past estimated symbols and D is the equalizer delay. Note that N_f and N_b also indicate the number of forward filter taps and feedback filter taps, respectively.

In Yukawa and Yamada (2009), a variable-metric adaptive projected subgradient algorithm (V-APSM) was developed to take advantage of the sparsity of equalizer. The original V-APSM algorithm is based on the MMSE criterion. In this paper we extend the V-APSM framework to DFE. Further, we design the DFE directly based on the minimum-SER criterion. The optimization problem is expressed as follows:

$$\min_{\mathbf{w}_k, \mathbf{b}_k} \left\{ \|\mathbf{w}_k - \mathbf{w}_{k-1}\|^2_{\mathbf{G}_{f,k}^{-1}} + \|\mathbf{b}_k - \mathbf{b}_{k-1}\|^2_{\mathbf{G}_{b,k}^{-1}} \right\} \tag{4}$$

$$s.t. \qquad Detec(y_k) = s_{k-D} \tag{5}$$

where $\|\mathbf{x}\|^2_{\mathbf{A}} = \mathbf{x}^T\mathbf{A}\mathbf{x}$ stands for the generalized inner product. $\mathbf{G}_{f,k}$ and $\mathbf{G}_{b,k}$ are real diagonal matrices called sparse matrices. $Detec(y_k)$ denotes the symbol detection operation on y_k. We shall force the equalizer to provide correct symbol detection, so as to minimize the symbol error rate.

3. Algorithm derivation

In this section we shall derive the DFE and the sparse matrix selection scheme. Without lost of generality, we consider 4-QAM

sources, the real and imaginary parts of the transmitted signal are drawn from $\{+1, -1\}$.

An adaptive equalizer updates the equalizer coefficients based on each received snapshot and its corresponding equalizer output. Note that the real and imaginary parts of the equalizer output are independent. We first derive the iterative formula based on the real part of the equalizer output. The real part of the equalizer output is given by

$$\Re\{y_k\} = \Re\left\{\mathbf{w}_k^T\mathbf{r}_k + \mathbf{b}_k^T\hat{\mathbf{s}}_k\right\} = \overline{\mathbf{w}}_k^T\overline{\mathbf{r}}_k + \overline{\mathbf{b}}_k^T\overline{\hat{\mathbf{s}}}_k, \tag{6}$$

where $\overline{\mathbf{w}}_k = [\mathbf{w}_R^T, -\mathbf{w}_I^T]^T$, $\overline{\mathbf{r}}_k = [\mathbf{r}_R^T, \mathbf{r}_I^T]^T$, $\overline{\mathbf{b}}_k = [\mathbf{b}_R^T, -\mathbf{b}_I^T]^T$ and, $\overline{\hat{\mathbf{s}}}_k = [\hat{\mathbf{s}}_R^T, \hat{\mathbf{s}}_I^T]^T$. Subscripts R and I denote the real and imaginary parts of the vector elements, respectively.

If consider only the real part of the equalizer output, the constraint of symbol detection can denote as $sgn(\Re\{y_k\}) = \Re\{s_{k-D}\}$. We can equivalently rewrite the constraint as follows:

$$\begin{cases} \mathrm{sgn}(\overline{\mathbf{w}}_k^T\overline{\mathbf{r}}_k + \overline{\mathbf{b}}_k^T\overline{\hat{\mathbf{s}}}_k - \Re\{s_{k-D}\} + 1) = 1 \\ \mathrm{sgn}(\overline{\mathbf{w}}_k^T\overline{\mathbf{r}}_k + \overline{\mathbf{b}}_k^T\overline{\hat{\mathbf{s}}}_k - \Re\{s_{k-D}\} - 1) = -1. \end{cases} \tag{7}$$

By combining (5), (6) and (7), we can obtain the optimization problem as follows:

$$\begin{aligned} \min_{\overline{\mathbf{w}}_k, \overline{\mathbf{b}}_k} \quad & \left\{ \left\|\overline{\mathbf{w}}_k - \overline{\mathbf{w}}_{k-1}\right\|^2_{\overline{\mathbf{G}}_{f,k}^{-1}} + \left\|\overline{\mathbf{b}}_k - \overline{\mathbf{b}}_{k-1}\right\|^2_{\overline{\mathbf{G}}_{b,k}^{-1}} \right\} \\ s.t. \quad & \mathrm{sgn}(\overline{\mathbf{w}}_k^T\overline{\mathbf{r}}_k + \overline{\mathbf{b}}_k^T\overline{\hat{\mathbf{s}}}_k - \Re\{s_{k-D}\} + 1) + \\ & \mathrm{sgn}(\overline{\mathbf{w}}_k^T\overline{\mathbf{r}}_k + \overline{\mathbf{b}}_k^T\overline{\hat{\mathbf{s}}}_k - \Re\{s_{k-D}\} - 1) = 0, \end{aligned} \tag{8}$$

where $\overline{\mathbf{G}}_{f,k}$ and $\overline{\mathbf{G}}_{b,k}$ are $2N_f \times 2N_f$ and $2N_b \times 2N_b$ diagonal matrices constructed from $\mathbf{G}_{f,k}$ and $\mathbf{G}_{b,k}$: $\overline{\mathbf{G}}_{f,k} = diag\{\mathbf{G}_{f,k}, \mathbf{G}_{f,k}\}$, $\overline{\mathbf{G}}_{b,k} = diag\{\mathbf{G}_{b,k}, \mathbf{G}_{b,k}\}$. We use $\tanh(\beta x)$ to approximate $\mathrm{sgn}(x)$ and apply the Lagrange multiplier method to solve the above optimization problem, where β is a positive constant to scale the input (Gong et al., 2013). Therefore, we can obtain the objective function as follows:

$$\begin{aligned} \boldsymbol{J}(\overline{\mathbf{w}}_k, \overline{\mathbf{b}}_k) = & \left\|\overline{\mathbf{w}}_k - \overline{\mathbf{w}}_{k-1}\right\|^2_{\overline{\mathbf{G}}_{f,k}^{-1}} + \left\|\overline{\mathbf{b}}_k - \overline{\mathbf{b}}_{k-1}\right\|^2_{\overline{\mathbf{G}}_{b,k}^{-1}} + + \\ & \eta\Big(\tanh(\beta(\overline{\mathbf{w}}_k^T\overline{\mathbf{r}}_k + \overline{\mathbf{b}}_k^T\overline{\hat{\mathbf{s}}}_k - \Re\{s_{k-D}\} + 1)) + + \\ & \tanh(\beta(\overline{\mathbf{w}}_k^T\overline{\mathbf{r}}_k + \overline{\mathbf{b}}_k^T\overline{\hat{\mathbf{s}}}_k - \Re\{s_{k-D}\} - 1))\Big), \end{aligned} \tag{9}$$

where η is the Lagrange multiplier. We set $\partial\boldsymbol{J}(\overline{\mathbf{w}}_k, \overline{\mathbf{b}}_k)/\partial\overline{\mathbf{w}}_k = 0$, and obtain

$$\overline{\mathbf{w}}_k = \overline{\mathbf{w}}_{k-1} - \frac{1}{2}\eta\beta[\tanh'(\beta(\Psi_R + 1)) + \tanh'(\beta(\Psi_R - 1))]\overline{\mathbf{G}}_{f,k}\overline{\mathbf{r}}_k, \tag{10}$$

where $\Psi_R = \overline{\mathbf{w}}_k^T\overline{\mathbf{r}}_k + \overline{\mathbf{b}}_k^T\overline{\hat{\mathbf{s}}}_k - \Re\{s_{k-D}\}$ $\tanh'(\cdot)$ is the derivative of $\tanh(\cdot)$. Substituting (10) into the constraint of (8) and using $\tanh(\beta x)$ to approximate $\mathrm{sgn}(x)$ in (8), we get (11) as follows:

$$\begin{aligned} & \tanh\left(\beta(\Omega_R + 1) - \frac{1}{2}\eta\beta^2[\tanh'(\beta(\Psi_R + 1)) + \tanh'(\beta(\Psi_R - 1))]\overline{\mathbf{r}}_k^T\overline{\mathbf{G}}_{f,k}^T\overline{\mathbf{r}}_k\right) + \tanh\left(\beta(\Omega_R - 1) - \frac{1}{2}\eta\beta^2[\tanh'(\beta(\Psi_R + 1)) \right. \\ & \left. + \tanh'(\beta(\Psi_R - 1))]\overline{\mathbf{r}}_k^T\overline{\mathbf{G}}_{f,k}^T\overline{\mathbf{r}}_k\right) = 0, \end{aligned} \tag{11}$$

where $\Omega_R = \overline{\mathbf{w}}_{k-1}^T\overline{\mathbf{r}}_k + \overline{\mathbf{b}}_k^T\overline{\hat{\mathbf{s}}}_k - \Re\{s_{k-D}\}$.

If the equalizer can primely compensate the channel distortion, the second item of $\tanh(\cdot)$ in (11) becomes a small value. Therefore, we can calculate (11) by using the first order Taylor series, i.e., $\tanh(x + \Delta) \approx \tanh(x) + \Delta\tanh'(x)$. Then we obtain the approximate expression of (11), as follows:

$$\begin{aligned} & \frac{1}{2}\eta\beta[\tanh'(\beta(\Psi_R + 1)) + \tanh'(\beta(\Psi_R - 1))] = \\ & \frac{\tanh(\beta(\Omega_R + 1)) + \tanh(\beta(\Omega_R - 1))}{\beta[\tanh'(\beta(\Omega_R + 1)) + \tanh'(\beta(\Omega_R - 1))]\overline{\mathbf{r}}_k^T\overline{\mathbf{G}}_{f,k}^T\overline{\mathbf{r}}_k}. \end{aligned} \tag{12}$$

If the channel has been well compensated, we will have $\overline{\mathbf{w}}_{k-1}^T\overline{\mathbf{r}}_k + \overline{\mathbf{b}}_k^T\overline{\hat{\mathbf{s}}}_k \approx \Re\{s_{k-D}\}$, that is $\Omega_R \approx 0$. So $\beta[\tanh'(\beta(\Omega_R + 1)) + \tanh'(\beta(\Omega_R - 1))] \approx 2\beta\tanh'(\beta)$ turns out to be a constant. At time slot k, $\overline{\mathbf{b}}_k$ is unknown, and we can use $\overline{\mathbf{b}}_{k-1}$ instead. Substituting (12) into (10) we obtain

$$\overline{\mathbf{w}}_k = \overline{\mathbf{w}}_{k-1} - \frac{\mu_f\overline{\mathbf{G}}_{f,k}\overline{\mathbf{r}}_k}{\overline{\mathbf{r}}_k^T\overline{\mathbf{G}}_{f,k}\overline{\mathbf{r}}_k}\Phi_R, \tag{13}$$

where $\Phi_R = [\tanh(\beta(\overline{\Omega}_R + 1)) + \tanh(\beta(\overline{\Omega}_R - 1))]$, $\overline{\Omega}_R = \overline{\mathbf{w}}_{k-1}^T\overline{\mathbf{r}}_k + \overline{\mathbf{b}}_{k-1}^T\overline{\hat{\mathbf{s}}}_k - \Re\{s_{k-D}\}$, μ_f indicates the impact of all scalars.

Similarly, set $\partial\boldsymbol{J}(\overline{\mathbf{w}}_k, \overline{\mathbf{b}}_k)/\partial\overline{\mathbf{b}}_k = 0$, and we can use similar method to derive the iteration formula corresponding to the imaginary part of the equalizer output.

$$\overline{\mathbf{b}}_k = \overline{\mathbf{b}}_{k-1} - \frac{\mu_b\overline{\mathbf{G}}_{b,k}^T\overline{\hat{\mathbf{s}}}_k^T}{\hat{\mathbf{s}}_k}\overline{\mathbf{G}}_{b,k}^T\overline{\hat{\mathbf{s}}}_k\Phi_R. \tag{14}$$

By combining Eqs. (13) and (14), we can get a complex form of the Proportional Minimum Symbol Error Rate (PMSER) algorithm, as follows:

$$\mathbf{w}_k = \mathbf{w}_{k-1} - \frac{\mu_f I_k}{\mathbf{r}_k^H\mathbf{G}_{f,k}^T\mathbf{r}_k}\mathbf{G}_{f,k}\mathbf{r}_k^* \tag{15}$$

$$\mathbf{b}_k = \mathbf{b}_{k-1} - \frac{\mu_b I_k}{\hat{\mathbf{s}}_k^H\mathbf{G}_{b,k}^T\hat{\mathbf{s}}_k\mathbf{G}_{b,k}\hat{\mathbf{s}}_k^*}, \tag{16}$$

where the iterative formulas in (15) and (16) have similar form to the IPNLMS algorithm in Pelekanakis and Chitre (2010). I_k is a complex error indicator of symbol detection defined as (Gong et al., 2013; Chen et al., 2017)

$$\begin{cases} \Re\{I_k\} = (\tanh(\beta(\overline{\Omega}_R + 1)) + \tanh(\beta(\overline{\Omega}_R - 1)))/2 \\ \Im\{I_k\} = (\tanh(\beta(\overline{\Omega}_I + 1)) + \tanh(\beta(\overline{\Omega}_I - 1)))/2. \end{cases} \tag{17}$$

4. Sparse matrix selection

To explore the sparsity of the equalizer, for the NLMS algorithm Rupp et al. (Rupp and Cezanne, 2000) illustrated that the matrix elements of $\mathbf{G}_{f,k}$, $\mathbf{G}_{b,k}$ should be proportional to the absolute values of the filter coefficients. Inspired by this work, next we discuss the sparse matrix selection of the proposed PMSER algorithm.

First, we assume that $\mathbf{w}^*$ and $\mathbf{b}^*$ correspond to the optimal filter vector of $\overline{\mathbf{w}}_k$ and $\overline{\mathbf{b}}_k$. Define $\widetilde{\mathbf{w}}_k = \overline{\mathbf{w}}_k - \mathbf{w}^*$ and $\widetilde{\mathbf{b}}_k = \overline{\mathbf{b}}_k - \mathbf{b}^*$ as the error vectors at slot k, respectively. Further we define the forward filter variance as $\mathbf{M}_k = E\left[\widetilde{\mathbf{w}}_k \widetilde{\mathbf{w}}_k^H\right]$, where $E[\cdot]$ denotes the statistical expectation and $[\cdot]^H$ denotes the conjugate transpose. Based on (13) we can present $\widetilde{\mathbf{w}}_k$ as

$$\widetilde{\mathbf{w}}_k = \widetilde{\mathbf{w}}_{k-1} - \frac{\mu_f \overline{\mathbf{G}}_{f,k} \overline{\mathbf{r}}_k \Phi_R}{\overline{\mathbf{r}}_k^T \overline{\mathbf{G}}_{f,k} \overline{\mathbf{r}}_k}. \tag{18}$$

Next we will simplify Φ_R. At slot $k-1$, we have $\widetilde{\mathbf{w}}_{k-1} = \overline{\mathbf{w}}_{k-1} - \mathbf{w}^*$ and $\widetilde{\mathbf{b}}_{k-1} = \overline{\mathbf{b}}_{k-1} - \mathbf{b}^*$, therefore we can obtain

$$\overline{\mathbf{r}}_k^T \widetilde{\mathbf{w}}_{k-1} = \overline{\mathbf{r}}_k^T \overline{\mathbf{w}}_{k-1} - \overline{\mathbf{r}}_k^T \mathbf{w}^* \tag{19}$$

$$\overline{\widetilde{\mathbf{s}}}_k^T \widetilde{\mathbf{b}}_{k-1} = \overline{\widetilde{\mathbf{s}}}_k^T \overline{\mathbf{b}}_{k-1} - \overline{\widetilde{\mathbf{s}}}_k^T \mathbf{b}^*. \tag{20}$$

We rewrite Φ_R as $\Phi_R = f(\rho_1) + f(\rho_2)$, where $f(x) = \tanh(\beta x)$ and

$$\begin{aligned} \rho_1 &= \overline{\mathbf{r}}_k^T \overline{\mathbf{w}}_{k-1} + \overline{\widetilde{\mathbf{s}}}_k^T \overline{\mathbf{b}}_{k-1} - \Re\{s_{k-D}\} + 1 \\ &= \overline{\mathbf{r}}_k^T \widetilde{\mathbf{w}}_{k-1} + \overline{\widetilde{\mathbf{s}}}_k^T \widetilde{\mathbf{b}}_{k-1} - e + 1, \end{aligned} \tag{21}$$

where $e = \Re\{s_{k-D}\} - (\overline{\mathbf{r}}_k^T \mathbf{w}^* + \overline{\widetilde{\mathbf{s}}}_k^T \mathbf{b}^*)$. Since $\overline{\mathbf{r}}_k^T \widetilde{\mathbf{w}}_{k-1} + \overline{\widetilde{\mathbf{s}}}_k^T \widetilde{\mathbf{b}}_{k-1} - e$ is a small value, by using the first-order Taylor series expansion we have

$$\begin{aligned} f(\rho_1) &= f\left(1 + \overline{\mathbf{r}}_k^T \widetilde{\mathbf{w}}_{k-1} + \overline{\widetilde{\mathbf{s}}}_k^T \widetilde{\mathbf{b}}_{k-1} - e\right) \\ &\approx 1 + f'(1)\left(\overline{\mathbf{r}}_k^T \widetilde{\mathbf{w}}_{k-1} + \overline{\widetilde{\mathbf{s}}}_k^T \widetilde{\mathbf{b}}_{k-1} - e\right) \end{aligned} \tag{22}$$

Then we define $\rho_2 = \overline{\mathbf{r}}_k^T \overline{\mathbf{w}}_{k-1} + \overline{\widetilde{\mathbf{s}}}_k^T \overline{\mathbf{b}}_{k-1} - \Re\{s_{k-D}\} - 1$. By using the same method we have

$$\begin{aligned} \Phi_R &= f(\rho_1) + f(\rho_2) \\ &\approx 2f'(1)\left(\overline{\mathbf{r}}_k^T \widetilde{\mathbf{w}}_{k-1} + \overline{\widetilde{\mathbf{s}}}_k^T \widetilde{\mathbf{b}}_{k-1} - e\right) \end{aligned} \tag{23}$$

Substitute (18) and (23) into $\mathbf{M}_k$ and we have

$$\begin{aligned} \mathbf{M}_k &= \mathbf{M}_{k-1} - \frac{\mathbf{M}_{k-1}\overline{\mathbf{G}}_{f,k} + \overline{\mathbf{G}}_{f,k}\mathbf{M}_{k-1}}{\mathrm{tr}\left(\overline{\mathbf{G}}_{f,k}\right)} + \frac{\overline{\mathbf{G}}_{f,k}^2}{\mathrm{tr}^2\left(\overline{\mathbf{G}}_{f,k}\right)}\sigma^2 \\ &+ \frac{\overline{\mathbf{G}}_{f,k}}{\mathrm{tr}\left(\overline{\mathbf{G}}_{f,k}\right)}[\mathrm{tr}(\mathbf{M}_{k-1})\mathbf{I} + \mathbf{M}_{k-1} - \mathrm{diag}(\mathbf{M}_{k-1})] \\ &\times \frac{\overline{\mathbf{G}}_{f,k}}{\mathrm{tr}\left(\overline{\mathbf{G}}_{f,k}\right)}, \end{aligned} \tag{24}$$

The diagonal elements of matrix $\mathbf{M}_k$ can be presented as

$$\begin{aligned} \mathbf{m}_k &= \left(\mathbf{I} - 2\frac{\overline{\mathbf{G}}_{f,k}}{\mathrm{tr}\left(\overline{\mathbf{G}}_{f,k}\right)} + \frac{\overline{\mathbf{G}}_{f,k}^2}{\mathrm{tr}^2\left(\overline{\mathbf{G}}_{f,k}\right)}\mathbf{1}\mathbf{1}^T\right)\mathbf{m}_{k-1} \\ &+ \frac{\overline{\mathbf{G}}_{f,k}^2}{\mathrm{tr}^2\left(\overline{\mathbf{G}}_{f,k}\right)}\mathbf{1}\sigma^2. \end{aligned} \tag{25}$$

where $\mathbf{I}$ is the $2N_f \times 2N_f$ identity matrix and $\mathbf{1}$ is the $2N_f \times 1$ vector with all entries equal 1. Now we investigate $m_k(i)$, which is the i-th element in vector $\mathbf{m}_k$. Based on (25), it can be observed that $m_k(i)$ is proportional to $\left(1 - \overline{g}_{f,k}(i)/\mathrm{tr}\left(\overline{\mathbf{G}}_{f,k}\right)\right)^2 m_{k-1}^2(i)$, where $\overline{g}_{f,k}(i)$ is the i-th element on the diagonal of matrix $\overline{\mathbf{G}}_{f,k}$. Since $m_k(i)$ represents the deviation between the filter tap and the optimal filter tap obtained at slot k, by choosing $\overline{g}_{f,k}(i)$ in proportion to $|m_{k-1}(i)|$ we can make $m_k(i)$ converge to zero more quickly. However $m_k(i)$ is usually unknown and larger tap values will result in larger errors. One possible alternative is to set $\overline{\mathbf{G}}_{f,k} \propto \mathrm{diag}(|\overline{w}_k|)$. That is, the diagonal elements of the sparse matrix are proportional to the absolute value of the estimated filter taps. In the same way, we can obtain $\overline{\mathbf{G}}_{b,k} \propto \mathrm{diag}\left(\left|\overline{b}_k\right|\right)$. By deriving the imaginary part of the equalizer, we can get similar conclusions. So in the iterative formula of the complex structure, we have $\mathbf{G}_{f,k}$ and $\mathbf{G}_{b,k}$ proportional to the absolute value of the filter tap. Next, we will use the conclusions derived above to guide the selection of sparse matrix elements.

Usually the selection of matrices $\mathbf{G}_{f,k}$ and $\mathbf{G}_{b,k}$ should take into account the sparseness of the equalizer (Das and Chakraborty, 2016). Then, we use sparseness measure of impulse response in (Hoyer, 2004):

$$S_k(\mathbf{h}_k) = \frac{L}{L - \sqrt{L}}\left\{1 - \frac{\|\mathbf{h}_k\|_1}{\sqrt{L}\left\|\mathbf{h}_k\right\|_2}\right\}, \tag{26}$$

where L is the length of $\mathbf{h}_k$. $\|\mathbf{h}_k\|_1$ and $|h_k|$ are the 1-norm of the impulse response and the absolute value of the l-th impulse response tap at slot k, respectively.

We can see that if $\mathbf{h}_k$ is a delta function, that is,

$$\mathbf{h}_k = \begin{cases} \pm\upsilon, & i = i_1 \\ 0, & 0 \le i \le L-1, i \ne i_1 \end{cases} \tag{27}$$

then we have $S_k = 1$. In addition, if $\mathbf{h}_k$ has a constant magnitude for each taps, we have $S_k = 0$.

We use formula (26) to calculate the sparseness measure of the equalizer and its adaptive update during iteration can be expressed as

$$\xi_{f,k} = \lambda_f \xi_{f,k-1} + (1-\lambda_f) S_k(\mathbf{w}_{k-1}), \tag{28}$$

where λ_f is the forgetting factor. Finally, we adopt the Lagrangian relaxation method to obtain $g_{f,k}(l)$:

$$g_{f,k}(l) = \frac{(1-\alpha_f)\xi_{f,k}}{2N_f} + \frac{(1+\alpha_f)|\mathbf{w}_{k-1}(l)|}{2\|\mathbf{w}_{k-1}\|_1}. \tag{29}$$

where α_f is a scale indicating the weighting effect of the two measures of equalizer sparsity. By adopting $\|\mathbf{w}_{k-1}\|_1$ and $|\mathbf{w}_{k-1}(l)|$ in calculating the step size, a larger step size is assigned to the forward filtering taps which have large absolute value, and vice-versa. In addition we use the sparseness measure of equalizer to avoid the step sizes become too large. This algorithm is named sparse control PMSER (SC-PMSER). In this way, we can speed up the convergence of the algorithm.

Using the same way, we can obtain the expression of $g_{b,k}(l)$:

$$g_{b,k}(l) = \frac{(1-\alpha_b)\xi_{b,k}}{2N_b} + \frac{(1+\alpha_b)|\mathbf{b}_{k-1}(l)|}{2\|\mathbf{b}_{k-1}\|_1}, \tag{30}$$

where $\xi_{b,k} = \lambda_b \xi_{b,k-1} + (1-\lambda_b) S_k(\mathbf{b}_{k-1})$. Similar to α_f, α_b is applied to combine the two measures of equalizer sparsity. Usually we set $\alpha_f = \alpha_b$.

5. Receiver structure

In order to confront the complicated and time-varying real-world underwater acoustic channel, we combine the proposed SC-PMSER-DFE algorithm with turbo receiving structure, digital phase-locked loop and time reversal technique (Xu et al., 2018). Fig. 1 shows our proposed receiver structure, where $\prod$ and $\prod^{-1}$ represent the interleaver and uninterleaver, respectively. $L_E(b_k|\mathbf{r})$ is the bit priori information and $L_E(x_k|\mathbf{r})$ is the external soft information. Readers can refer to (Xu et al., 2018) for more detail of the turbo receiver.

We use the decision feedback equalization technique combined with the time reversal technique in Balakrishnan and Johnson (2000), where the output of the normal equalizer, denoted as $\widehat{s}_{1,k}$, and the output of the time reversal equalizer, denoted as $\widehat{s}_{2,k}$, are combined as follows:

$$\widehat{s}_k = \tau \widehat{s}_{1,k} + (1-\tau)\widehat{s}_{2,k}, \tag{31}$$

where we choose $\tau = 1/2$.

In order to counter the Doppler effect of the underwater acoustic channel, we apply the second-order digital phase-locked loop in Stojanovic et al. (1994) (shown in Fig. 2), where the output of the forward filter is $p_k = (\mathbf{w}_{f,k}^T \mathbf{r}_k) e^{-j\widehat{\theta}}$ and the output of the feedback filter is $q_k = \mathbf{w}_{b,k}^T \widetilde{\mathbf{d}}_k$, $\widetilde{\mathbf{d}}_k = \left[\widetilde{d}_{k-1}, \ldots, \widetilde{d}_{k-N_b}\right]^T$ is the previously detected symbol sequence. We can obtain the estimated value of the current symbol and estimated error as follows:

$$\widehat{d}_k = p_k - q_k \tag{32}$$

$$e_k = d_k - \widehat{d}_k \tag{33}$$

By using the MMSE criterion to minimizes the objective function $E\left[|e_k|^2\right]$, we obtain the following second-order DPLL.

$$\Phi_k = Im\{p_k (d_k + q_k)^*\} \tag{34}$$

$$\widehat{\theta}_{k+1} = \widehat{\theta}_k + K_{f_1}\Phi_k + K_{f_2}\sum_{i=0}^{k}\Phi_i \tag{35}$$

where K_{f_1} and K_{f_2} are tracking constants.

It is worth mentioning that we have adopted the reception diversity technique of equal-gain combination. Assume there are U hydrophones to receive the arriving signal. Each individual received signal is processed with the above mentioned turbo received and then combined with equal gains. That is,

$$\widehat{s}_k = \frac{1}{U}\sum_{u=1}^{U}\widehat{s}_k^u. \tag{8}$$

where $\widehat{s}_k^u$ denotes the received signal at the uth hydrophone.

6. Evaluations

Information sources are transmitted through UACs, where both simulated channel and real-world channels are applied. Furthermore, both training (TR) mode and Decision Direct (DD) mode are considered. In the TR mode, training symbols known to the receiver are first applied to update the DFE. Then, in the DD mode, the outputs of equalizer are applied to replace the actual symbols. The proposed algorithm is evaluated via a simulated acoustic channel and real-world field experiments. In the simulated channel, we evaluate the adaptive decision feedback equalizer (i.e. the turbo structure is not applied). In the field experiments, the turbo receiver is applied to tackle more complicated real-world channels.

For the proposed algorithm, we set $\beta = 1$, $\lambda_f = \lambda_b = 0.1$ and $\alpha_f = \alpha_b = -0.5$. Note that the selection of these parameters are based on the tradeoff between convergence speed and steady-state performance. Here we adopt some typical values applied in existing work. More discussion of the proper selection of the parameter were provided in the literature (Gong et al., 2013; Yukawa and Yamada, 2009; Das and Chakraborty, 2016).

6.1. Simulated channel

In the simulation, information sources are modulated by 4QAM modulation scheme. We apply the underwater channel model in Song et al. (2011). The real and imaginary parts of the complex underwater acoustic channel are plot in Fig. 3. The channel was sampled with sampling rate of 2500/s. Here a relative low sampling rate is applied such that the channel exhibits more obvious sparsity. We perform computer simulations to evaluate the uncoded Symbol Error Rate (SER) performance of the proposed SC-PMSER-DFE, and compare it with the IPNLMS-DFE algorithm that is based on the

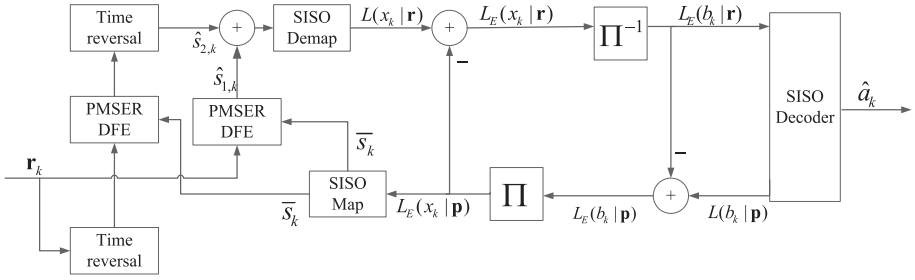

Fig. 1. Receiver structure with SC-PMSER-DFE.

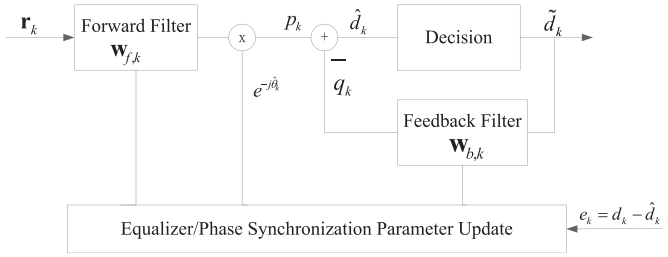

Fig. 2. DPLL combined with decision feedback equalizer.

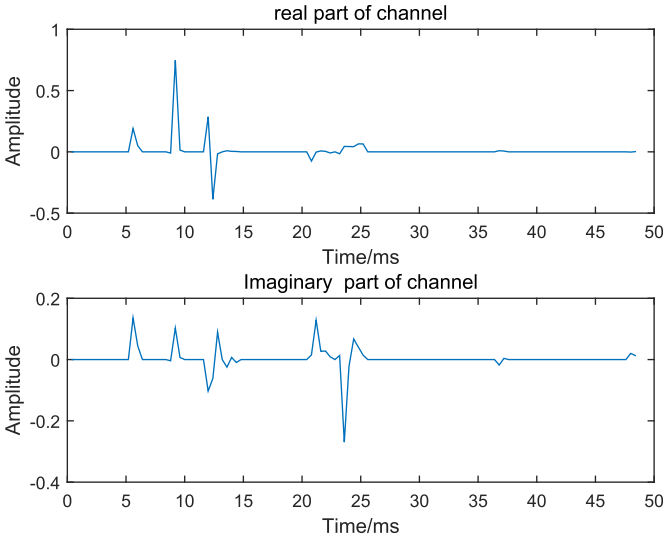

Fig. 3. CHANNEL 1: The complex impulse response generated from the channel model in Song et al. (2011).

Table 1
Parameters of equalizers.

	IPNLMS-DFE	MSER-DFE	SC-PMSER-DFE
TR mode	$\mu_f = 0.15$, $\mu_b = 0.25$		
DD mode	$\mu_f = \mu_b = 0.03$		
Number of taps	$N_f = N_b = 120$		

MMSE criterion and the MSER-DFE algorithm that does not exploit the sparsity of the equalizer.

In practical systems, the length of training sequence is usually limited. So we set the training sequence length to 1000. Table 1 presents the parameters of all equalizers. Note that we adopt smaller step sizes in the DD mode. This is because in DD mode the detected symbols, which may contain erotic detections, are applied as training symbols. A smaller step size can reduce the impact of erotic detection. Usually the length of the equalizer should be larger than that of the channel response. In this simulation we use large equalizer lengths to guarantee that they are larger than the channel responses.

Figs. 4 and 5 show the convergence curves of the three algorithms when SNR = 17 dB and SNR = 22 dB, respectively. It can be seen that SC-PMSER-DFE achieves better convergence performance than MSER-DFE and IPNLMS-DFE. Because the MSER algorithm has fewer errors at the beginning, our algorithm accumulates advantages in the next equilibrium, and accelerates the equalization by using sparsity. After the TR mode, due to the slow convergence of MSER-DFE, it suffer from the problem of error propagation.

Fig. 6 shows the SER curve of three algorithms corresponding to different SNRs. When the SNR is equal to 20 and 22 dB, in the simulation the proposed SC-PMSER DF equalizer results in zero

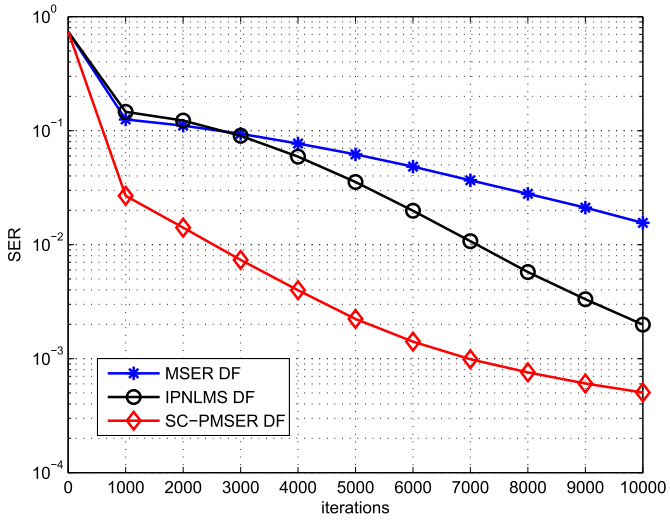

Fig. 4. Convergence curve of the three algorithms in CHANNEL 1, where SNR is fixed to 17 dB.

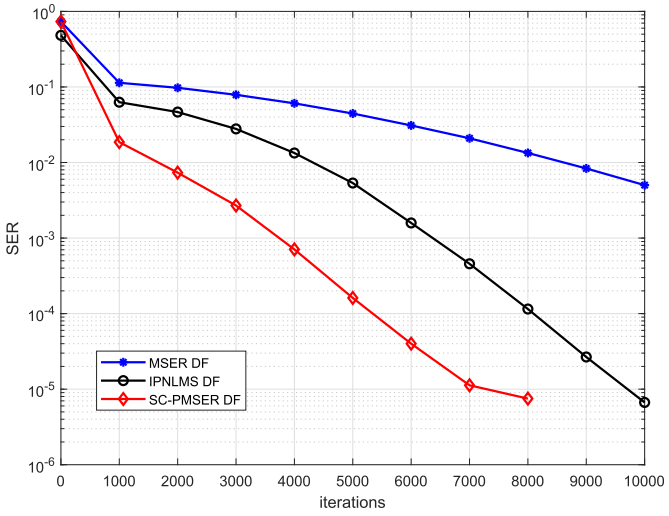

Fig. 5. 1.00,0.00,0.00Convergence curve of the three algorithms in CHANNEL 1, where SNR is fixed to 22 dB.

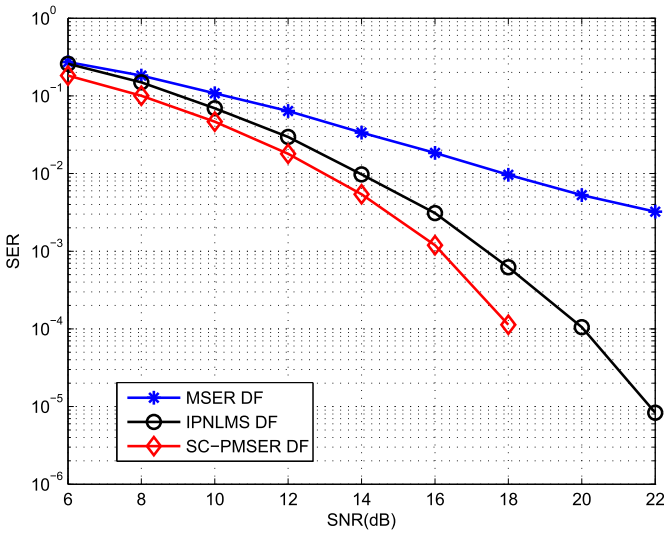

Fig. 6. SER performance of the three algorithms in CHANNEL 1.

erotic symbol detection. Hence no results were shown in Fig. 6. It can be observed that the SC-PMSER-DFE algorithms outperform MSER-DFE at all SNRs.

6.2. Real field experiment

We use our algorithm to decode the experimental data from a real-field test in the Thousand-island lake (Xu et al., 2018). The transmission data were modulated by 4-QAM modulation scheme and we used a recursive convolution code with a code rate of 1/2 and a polynomial of $[\mathbf{G}_1, \mathbf{G}_2]$= (Cotter and Rao, 2002; Benesty and Gay, 2002). The data rate is 6 Kbps. The center carrier frequency is 12 kHz and the sampling frequency is 96 kHz. Total transmission data were divided into 69 data frames. We added a falling Hyperbolic Frequency Modulation (HFM) signal in front of all the data frames for data synchronization. The rising HFM signal is added in each data frame for synchronization and doppler compensation. Based on the HFM signal, conventional double correlators can be applied to estimate the starting point and Doppler shift of each data frame (Wang et al., 2015) (Readers can refer to (Wang et al., 2015) for more detail of HFM signals).

The field experiments were carried out in the Thousand-island lake in Zhejiang province, China. Dipping transformers were placed 10 m under the water surface. The test scenario is shown in Fig. 7. Both static and mobile communication tests were carried out in the field experiment. The estimated channels based on known source signals are shown in Figs. 7 and 9. Fig. 7 is the channel impulse response obtained in an experiment conducted by a transmitter with a speed of 7.4 knots approaching the receiver. Fig. 9 shows the channel impulse responses when the transmitter and receiver are 700 m apart in winter. It can be seen that the channel impulse responses are gradually becoming sparse. We also note that Figs. 7 and 9 are not estimated by the proposed algorithm. They are obtained with the conventional least square method, to demonstrate the channel properties.

At the receiving end, we use the turbo equalization to process the received data. In turbo equalization, we compare the performance of IPNLMS DFE, MSER-DFE and SC-PMSER-DFE, Table 2 shows the parameters of the three equalizers.

Figs. 8 and 10 show the Bit Error Rate of all data frames which were processed by multiple turbo receivers. In Figs. 8 and 10 we compare the proposed SC-PMSER DFE turbo receiver with the

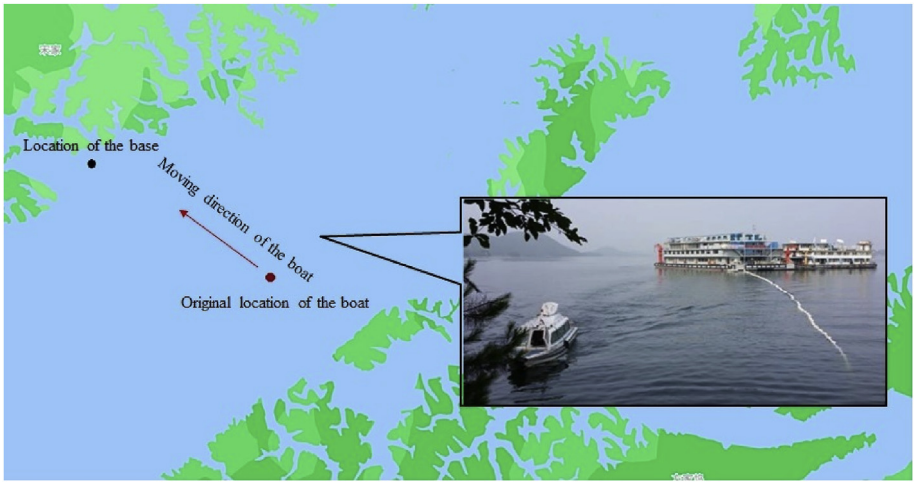

Fig. 7. Illustration of the field test in the Thousand-island, Zhejiang province, China.

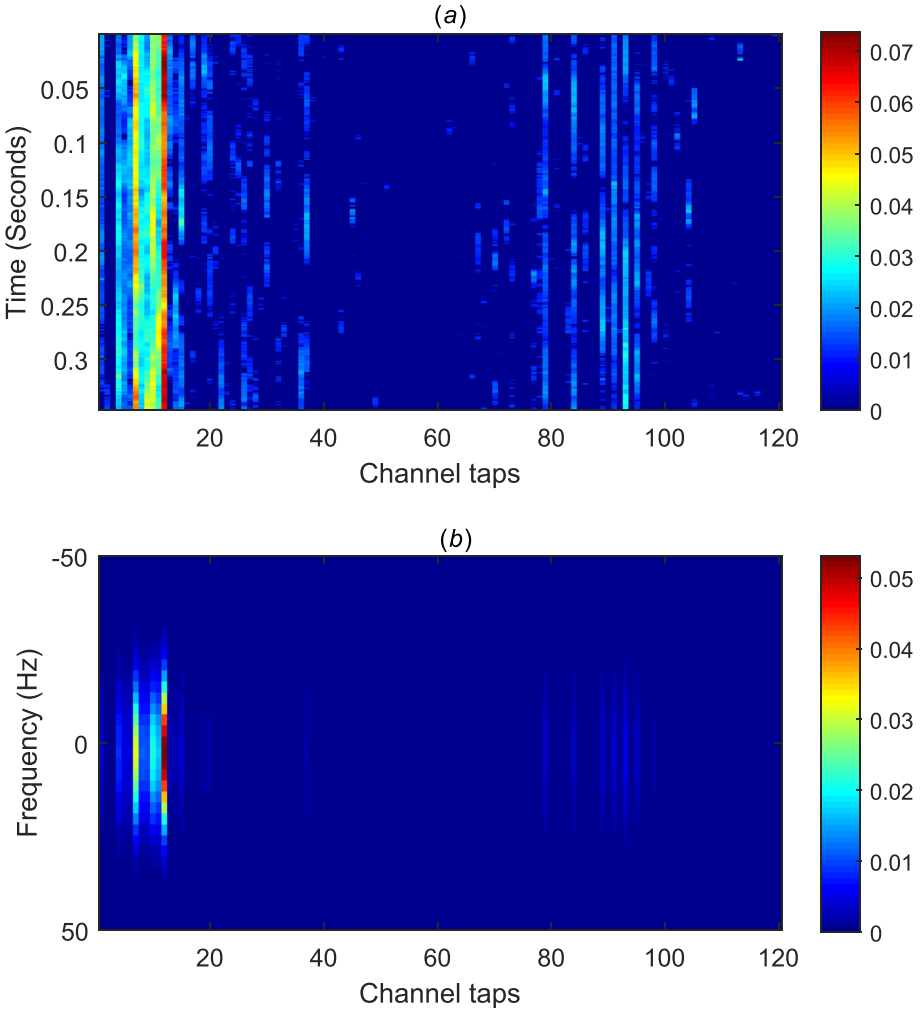

Fig. 8. CHANNEL 2: The transmitter approaches the receiver at 7.4 knots in the Thousand-island lake. (a) Time-domain channel response, (b) The Doppler spectrum.

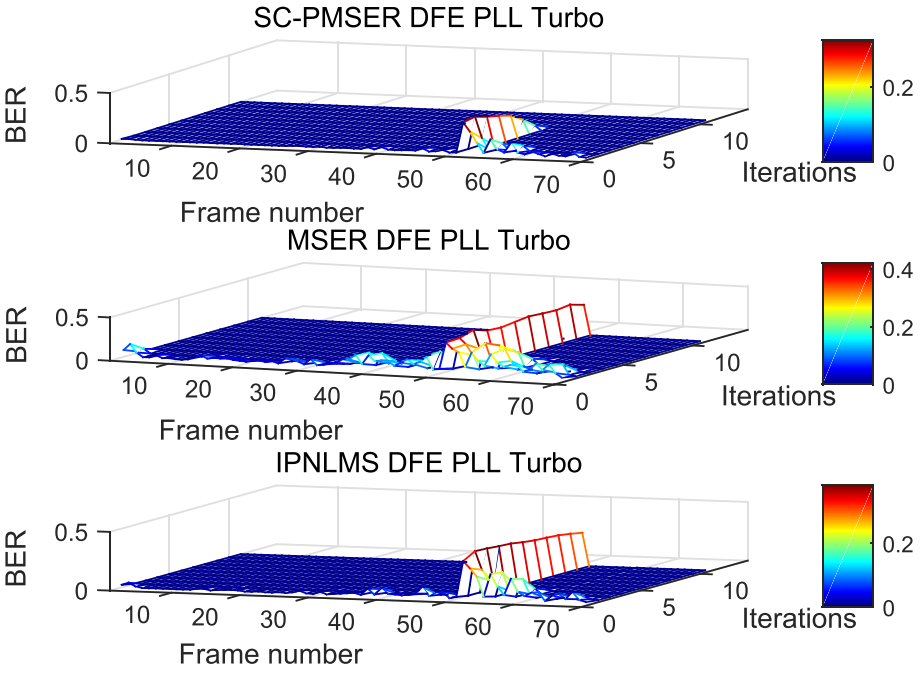

Fig. 9. Demodulation results of the algorithms under CHANNEL 2.

Table 2
Parameters of equalizers.

Algorithm	SC-PMSER-DFE		MSER-DFE		IPNLMS-DFE	
Filter type	Forward	Feedback	Forward	Feedback	Forward	Feedback
TR mode	$\mu_f = 0.6$	$\mu_b = 0.1$	$\mu_f = 0.6$	$\mu_b = 0.1$	$\mu_f = 0.6$	$\mu_b = 0.1$
DD mode	$\mu_f = 0.6$	$\mu_b = 0.1$	$\mu_f = 0.6$	$\mu_b = 0.1$	$\mu_f = 0.6$	$\mu_b = 0.1$
Number of taps	$N_f = 120$	$N_b = 51$	$N_f = 120$	$N_b = 51$	$N_f = 120$	$N_b = 51$

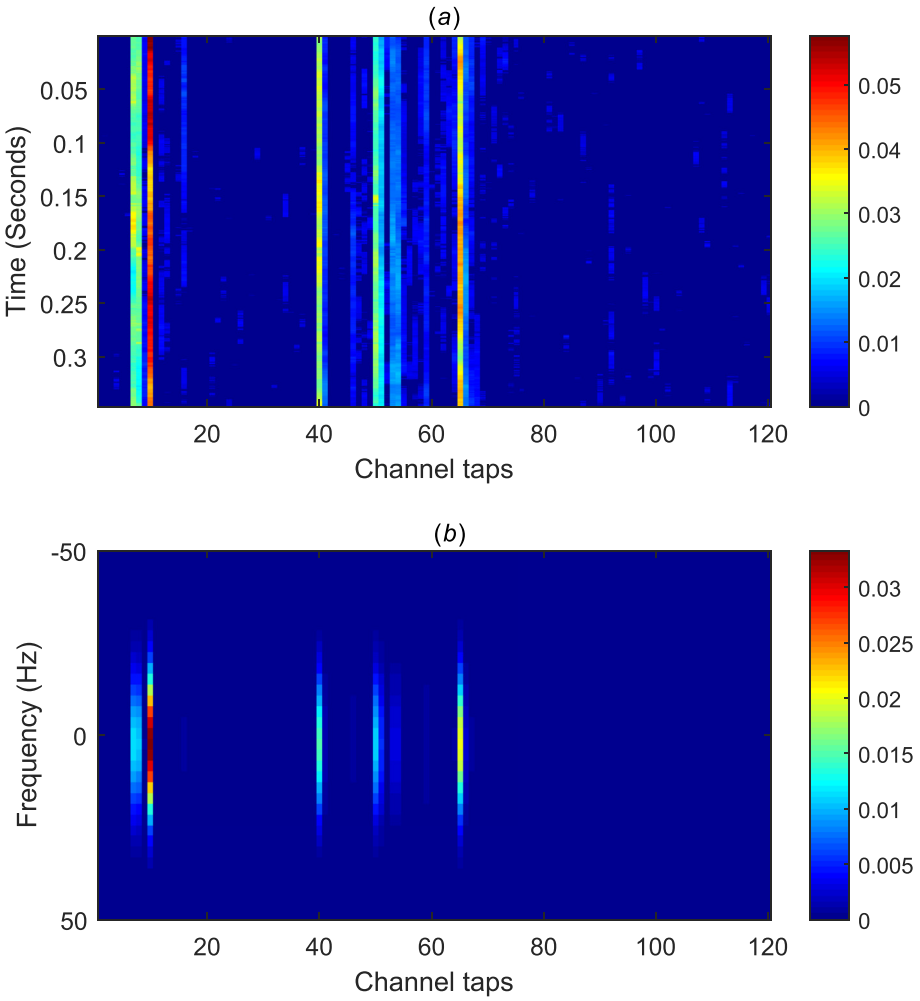

Fig. 10. CHANNEL 3: In the winter, the transceiver is 700 m apart in the Thousand-island lake. (a) Time-domain channel response, (b) The Doppler spectrum.

MSER DFE turbo receiver (Chen et al., 2017) that does not exploit the equalizer sparsity and the IPNLMS DFE turbo receiver that is based on the MMSE criterion. It can be observed that the proposed receiver requires fewer turbo iterations to obtain a converged result. For the 51st data frame, the BER quickly converges to zero when the data are processed by the proposed SC-PMSER DFE turbo receiver. While the results of the MSER DFE turbo receiver and the IPNLMS DFE turbo receiver cannot converge. Compared with CHANNEL 2, CHANNEL 3 exhibits much more obvious sparsity. Hence the sparsity based schemes show superior performance. Moreover, it can be observed that the proposed algorithm exhibits faster convergence speed than the MSER DFE turbo receiver and the IPNLMS DFE turbo receiver (see Fig. 11).

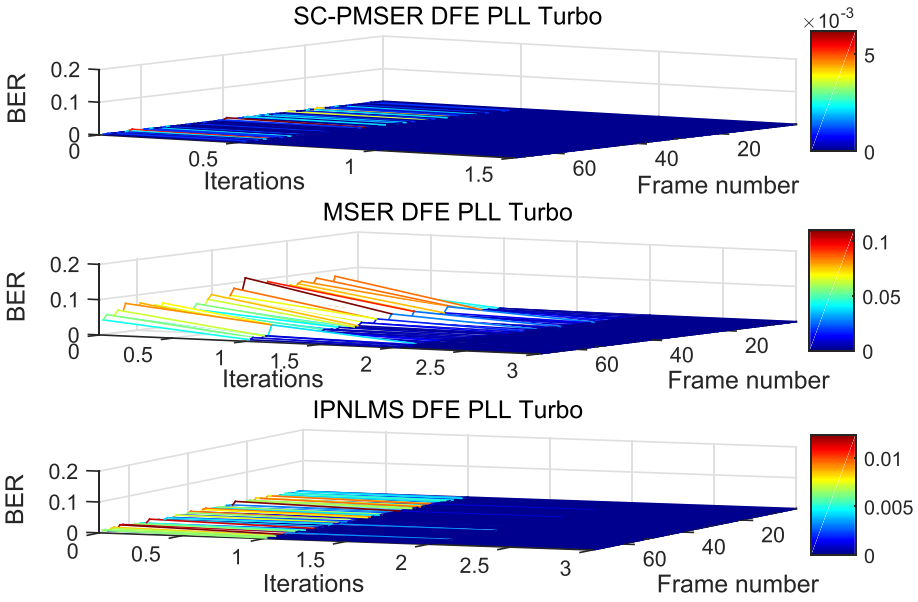

Fig. 11. Demodulation results of the algorithms under CHANNEL 3.

7. Conclusion

Based on our previously proposed MSER-DFE scheme, we have proposed an improved DFE which exploits the sparsity of the equalizer. Compared to the original MSER-DFE, our new algorithm assigns independent step sizes to the equalizer taps, thus achieves faster convergence speed. The selection scheme of the time-varying step size, i.e. the sparse matrices, is also provided. Furthermore, we propose a receiver structure that combines SC-PMSER-DFE with turbo decoding, DPLL, time reversal diversity and multi-reception diversity. We use this receiver to demodulate signals received under different sparse channels. The demodulation results show that our new algorithm can effectively reduce the number of turbo iterations and accelerate the convergence of the receiver.

Declaration of competing interest

The authors declare that they have no known competing financial interests or personal relationships that could have appeared to influence the work reported in this paper.

Acknowledgments

This work was supported in part by the National Natural Science Foundation of China under Grants U1701265 and in part by Key Program of Marine Economy Development(Six Marine Industries) Special Foundation of Department of Natural Resources of Guangdong Province(GDNRC [2020]009)

References

Balakrishnan, J., Johnson Jr., C.R., 2000. Time-reversal diversity in decision feedback equalization. In: Proc. Of Allerton Conf. on Comm. Control and Computing. Citeseer.

Benesty, J., Gay, S.L., May. 2002. An improved PNLMS algorithm. In: 2002 IEEE International Conference on Acoustics, Speech, and Signal Processing, vol. 2. IEEE. II–1881.

Chen, S., Hanzo, L., Mulgrew, B., 2004. Adaptive minimum symbol-error-rate decision feedback equalization for multilevel pulse-amplitude modulation. IEEE Trans. Signal Process. 52 (7), 2092–2101.

Chen, S., Hanzo, L., Livingstone, A., 2006. Mber space-time decision feedback equalization assisted multiuser detection for multiple antenna aided sdma systems. IEEE Trans. Signal Process. 54 (8), 3090–3098.

Chen, F., Lin, S., Zheng, B., Li, Q., Wen, M., Liu, Y., Ji, F., 2017. Minimum symbol-error rate based adaptive decision feedback equalizer in underwater acoustic channels. IEEE Access 5, 25147–25157. https://doi.org/10.1109/ACCESS.2017.2772302.

Chen, S., Tan, S., Xu, L., Hanzo, L., Jul. 2008. Adaptive minimum error-rate filtering design: a review. Signal Process. 88 (7), 1671–1697.

Cotter, S.F., Rao, B.D., Aug. 2002. Sparse channel estimation via matching pursuit with application to equalization. IEEE Trans. Commun. 50 (3), 374–377.

Das, R.L., Chakraborty, M., Apr. 2016. Improving the performance of the PNLMS algorithm using l_1 norm regularization. IEEE/ACM Trans. Audio Speech Lang. Process. (TASLP) 24 (7), 1280–1290.

Duan, W., Tao, J., Zheng, Y.R., 2017. Efficient adaptive turbo equalization for multiple-input–multiple-output underwater acoustic communications. IEEE J. Ocean. Eng. 43 (3), 792–804.

Duttweiler, D.L., Sep. 2000. Proportionate normalized least-mean-squares adaptation in echo cancelers. IEEE Trans. Speech Audio Process. 8 (5), 508–518.

Feng, X., et al., 2012. Sparse Equalizer Filter Design for Multi-Path Channels. Massachusetts Institute of Technology. Ph.D. thesis.

Gong, M., Chen, F., Yu, H., Lu, Z., Hu, L., Feb. 2013. Normalized adaptive channel equalizer based on minimal symbol-error-rate. IEEE Trans. Commun. 61 (4), 1374–1383.

Hoyer, P.O., Nov 2004. Non-negative matrix factorization with sparseness constraints. J. Mach. Learn. Res. 5, 1457–1469.

Kocic, M., Brady, D., Stojanovic, M., 1995. Sparse equalization for real-time digital underwater acoustic communications. In: 'Challenges of Our Changing Global Environment'. Conference Proceedings, vol. 3. OCEANS'95 MTS/IEEE, pp. 1417–1422. IEEE.

Liu, L., Sun, D., Zhang, Y., 2017. A family of sparse group lasso rls algorithms with adaptive regularization parameters for adaptive decision feedback equalizer in the underwater acoustic communication system. Phys. Commun. 23, 114–124.

Pelekanakis, K., Chitre, M., Nov. 2010. Comparison of sparse adaptive filters for underwater acoustic channel equalization/estimation. In: 2010 IEEE International Conference on Communication Systems. IEEE, pp. 395–399.

Pelekanakis, K., Chitre, M., 2012. New sparse adaptive algorithms based on the natural gradient and the $l0$-norm. IEEE J. Ocean. Eng. 38 (2), 323–332.

Qingwei, M., Jianguo, H., Jing, H., Chengbing, H., Chuang, M., 2012. An improved direct adaptive multichannel turbo equalization scheme for underwater communications. In: 2012 Oceans-Yeosu. IEEE, pp. 1–5.

Rupp, M., Cezanne, J., 2000. Robustness conditions of the lms algorithm with time-variant matrix step-size. Signal Process. 80 (9), 1787–1794.

Singer, A.C., Nelson, J.K., Kozat, S.S., 2009. Signal processing for underwater acoustic communications. IEEE Commun. Mag. 47 (1), 90–96.

Song, A., Senne, J., Badiey, M., Smith, K.B., 2011. Underwater acoustic communication channel simulation using parabolic equation. In: Proceedings of the Sixth ACM International Workshop on Underwater Networks. ACM, 2:1–2:5.

Stojanovic, M., Preisig, J., Feb. 2009. Underwater acoustic communication channels: propagation models and statistical characterization. IEEE Commun. Mag. 47 (1), 84–89.

Stojanovic, M., Catipovic, J.A., Proakis, J.G., 1994. Phase-coherent digital communications for underwater acoustic channels. IEEE J. Ocean. Eng. 19 (1), 100–111.

Tao, J., An, L., Zheng, Y.R., 2017. Enhanced adaptive equalization for mimo underwater acoustic communications. In: OCEANS 2017-Anchorage. IEEE, pp. 1–5.

Wang, K., Chen, S., Liu, C., Liu, Y., Xu, Y., 2015. Doppler estimation and timing synchronization of underwater acoustic communication based on hyperbolic frequency modulation signal. In: 2015 IEEE 12th International Conference on Networking. Sensing and Control, pp. 75–80. https://doi.org/10.1109/ICNSC.2015.7116013.

Wu, Y., Zhu, M., Li, X., 2015. Sparse linear equalizers for turbo equalizations in underwater acoustic communication. In: OCEANS 2015-MTS/IEEE Washington. IEEE, pp. 1–6.

Xu, L., Zhong, X., Yu, H., Chen, F., Ji, F., Yan, S., Feb. 2018. Spatial and time-reversal diversity aided least-symbol-error-rate turbo receiver for underwater acoustic communications. IEEE Access 6, 9049–9058. https://doi.org/10.1109/ACCESS.2018.2805816.

Yukawa, M., Yamada, I., Dec. 2009. A unified view of adaptive variable-metric projection algorithms. EURASIP J. Adv. Signal Process. 2009 34.

Zheng, B., Chen, F., Ji, F., Yu, H., Nov. 2013. Least-symbol-error-rate adaptive decision feedback equalization for underwater channel. In: Proceedings of the Eighth ACM International Conference on Underwater Networks and Systems. ACM, p. 41.